Measurement of the $2S_{1/2} - 8D_{5/2}$ Transition in Hydrogen

A. D. Brandt,[1] S. F. Cooper,[1] C. Rasor,[1] Z. Burkley,[1] A. Matveev,[2] and D. C. Yost[1,*]
[1]Department of Physics, Colorado State University, Fort Collins, Colorado 80523, USA
[2]Russian Quantum Center, Skolkovo, Moscow 143025, Russia

(Received 26 September 2021; revised 15 November 2021; accepted 7 December 2021; published 13 January 2022)

We present a measurement of the hydrogen $2S_{1/2} - 8D_{5/2}$ transition performed with a cryogenic atomic beam. The measured resonance frequency is $\nu = 770649561570.9(2.0)$ kHz, which corresponds to a relative uncertainty of 2.6×10^{-12}. Combining our result with the most recent measurement of the $1S - 2S$ transition, we find a proton radius of $r_p = 0.8584(51)$ fm and a Rydberg constant of $R_\infty = 10973731.568332(52)$ m^{-1}. This result has a combined 3.1σ disagreement with the Committee on Data for Science and Technology (CODATA) 2018 recommended value.

DOI: 10.1103/PhysRevLett.128.023001

Spectroscopy of hydrogen, the simplest element, was pivotal in the development of quantum theory and now plays a crucial role in the determination of fundamental constants and precision tests of fundamental theory [1–3]. Because of its simplicity, theoretical calculations of the energy levels of hydrogen can be made with high accuracy, and deviations from theoretical predictions could suggest the presence of new physics [4–8].

The energy levels of hydrogen can be described by the following expression, given by Refs. [9,10]:

$$E_{n,l,j} = hcR_\infty \left[-\frac{1}{n^2} + f_{n,l,j}\left(\alpha, \frac{m_e}{m_p}, \ldots\right) + \delta_{l,0}\frac{k_N}{n^3} r_p^2 \right]. \quad (1)$$

The first term, which depends only on the principle quantum number n, is the gross structure contribution from nonrelativistic quantum theory. The second term accounts for quantum electrodynamics (QED) and relativistic recoil corrections [3,11]. The last term is the leading correction to the S states arising from the finite size of the nucleus, where r_p is the root mean square charge radius of the proton. By measuring two hydrogen transitions, the Rydberg constant, R_∞, and r_p in Eq. (1) can be determined. While $f_{n,l,j}$ is a function of other physical constants, such as the fine-structure constant and electron-to-proton mass ratio, each of these have been measured with sufficient precision in other experiments to not limit the determination of R_∞ and r_p. Therefore, assuming that the QED corrections are accurately applied, a consistent extraction of R_∞ and r_p from spectroscopic measurements is expected.

Tension arose when the value of r_p obtained from muonic hydrogen was compared to the value determined from hydrogen spectroscopy and electron-proton elastic scattering data. This led to the "proton-radius puzzle" [12–15]. This discrepancy has spurred further interest in precision spectroscopy on hydrogen, and several new results have been recently published [9,10,16,17].

The Committee on Data for Science and Technology (CODATA) 2014 recommended r_p value, which is historically significant in the discussion of the proton-radius puzzle, is strongly influenced by previous measurements of the two-photon $2S - 8S/D$ transitions [18–20]. While remeasuring any of these transitions produces data relevant to the proton radius puzzle, the $2S_{1/2} - 8D_{5/2}$ transition is particularly attractive as it possesses the largest two-photon matrix element. Therefore, we have remeasured the $2S_{1/2} - 8D_{5/2}$ transition and report a value that has a 3 times smaller uncertainty as compared with the previous best measurement [19].

Our measurement has benefited from several technological advances. Improvements in laser technology afford us both the optical frequency comb to determine absolute optical frequencies and the ability to optically excite a sufficient population of hydrogen atoms to the metastable 2S state, as in Ref. [9]. By generating metastable atoms optically via the two-photon $1S_{1/2} - 2S_{1/2}$ transition, instead of by electron bombardment, we are able to perform spectroscopy on a cryogenic beam of hydrogen atoms, reducing velocity-dependent systematics and allowing for the selective population of the $2S_{1/2}^{F=1}$ hyperfine manifold. Therefore, optical production of an appreciable flux of metastable hydrogen represents a substantial improvement over previous measurements of this transition. We have also directly characterized the velocity distribution, reducing uncertainty in velocity-related systematics [21]. Additionally, our apparatus provides a geometrically constrained interaction between the hydrogen atoms and the spectroscopy light.

Our experimental apparatus has not been fully described elsewhere. We generate a cryogenic beam of hydrogen by disassociating molecular hydrogen in a microwave

discharge followed by a cryogenic nozzle [21]. At a distance of 1.5 m away from the nozzle, the atoms interact with 243 nm radiation to generate $2S_{1/2}^{F=1}$ population. The 243 nm radiation [22] is enhanced in an in-vacuum optical cavity [23] at a 6° angle from the atomic beam. The UV cavity mirrors are kept in a ~200 mTorr oxygen environment to prevent UV degradation, and a pair of differential pumping manifolds separates the mirror chambers from the spectroscopy region. The metastable 2S atoms then travel 15 cm before intersecting with 778 nm spectroscopy light from a Coherent-899 Ti:sapphire ring laser, which is also enhanced in an in-vacuum optical cavity at a 6° angle from the atomic beam. The linearly polarized 778 nm radiation excites the $2S_{1/2} - 8D_{5/2}$ transition. Population in the $8D_{5/2}$ state will rapidly decay—predominantly to the 2P state which will then decay to the 1S ground state. Therefore, by driving the $2S_{1/2} - 8D_{5/2}$ transition, we effectively quench the metastable population. The entire spectroscopic volume is within a pair of concentric magnetic shields, which is itself inside of a Faraday cage to mitigate Zeeman shifts and dc Stark shifts. The remaining metastable population not quenched by the 778 nm radiation is detected 15 cm past the $2S_{1/2} - 8D_{5/2}$ interaction volume by a channel electron multiplier. The absolute frequencies of the 243 and 778 nm radiation are determined by phase locking the lasers to a coherent Er fiber optical frequency comb whose repetition rate is continuously counted by a GPS-disciplined, Rb time base and whose f_0 beat note is phase locked to a rf synthesizer. See Fig. 1 for a schematic of our experimental apparatus.

The UV-enhancement cavity is about 1.8 m long and is constructed with a pair of 1 m radius of curvature mirrors—the effective $1/e^2$ beam radius is approximately 150 μm at the intersection with the atomic beam. Between 1% and 10% of atoms in the excitation volume are driven to the $2S_{1/2}^{F=1}$ state. The spectroscopy light is also enhanced in an in-vacuum optical cavity to drive appreciable population to the $8D_{5/2}$ state and the optical power is measured by continuously monitoring the cavity transmission with a photodiode.

A direct digital synthesizer (DDS) sets the beat frequencies between the comb and the other laser systems—the DDS itself is referenced to a 10 MHz signal from a GPS-disciplined, Rb time standard. To verify that our absolute frequency calibration is accurate, we locally counted a cesium-referenced 5 MHz signal at the NIST WWVB station in Fort Collins, Colorado, with the Rb time base and frequency counter, finding an accuracy within the expectations of a GPS-disciplined oscillator [24] (a fractional accuracy of $\approx 5 \times 10^{-13}$).

To scan the $2S_{1/2} - 8D_{5/2}$ transition, a set of 25 evenly spaced frequencies in a 3 MHz span around the resonance is chosen. This set of 25 frequency points is randomly sequenced. For each scan of the line, we fit the measured line shape with

$$\mathcal{F} = A \exp(-\alpha[\mathcal{L}_2(\nu_c, \gamma) + \mathcal{L}_3(\nu_c, \gamma)]), \tag{2}$$

where $\mathcal{L}_i$'s correspond to Lorentzian functions of appropriate relative magnitude centered on the $F = i$ hyperfine manifold, and $\{\alpha, \gamma, \nu_c\}$ are fit parameters for the amplitude of the metastable decrease, linewidth, and effective centroid frequency, respectively. Further details on the fitting function and other possible line shape distortions (including quantum interference [25]) can be found in the Supplemental Material (SM) [26].

We have developed numeric line shape models, which take into account the geometry and dynamics of the atom-light interaction, ac and dc Stark effects, velocity distribution, repopulation of the metastable state, and the

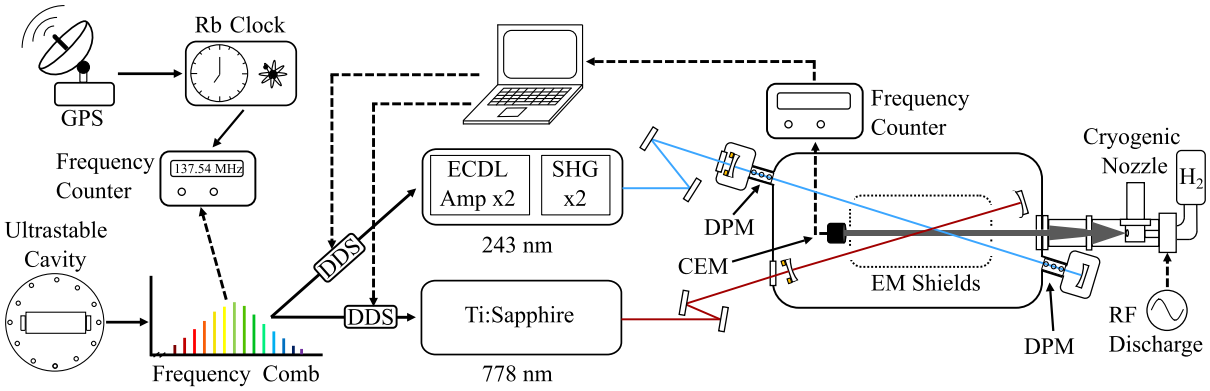

FIG. 1. Schematic of experiment. The repetition rate of the coherent frequency comb referenced to an ultrastable optical cavity is counted by a GPS-disciplined rubidium time standard. The 243 and 778 nm lasers are phase locked to the comb, with the beat frequency set by a direct digital synthesizer (DDS). The Ti:sapphire laser is a Coherent-899 vertically oriented ring laser with a modified piezoelectric controlled mirror to increase the frequency locking bandwidth. ECDL, extended cavity diode laser; SHG, second-harmonic generation; DPM, differential pumping manifolds; CEM, channel electron multiplier; EM shields, a pair of coaxial magnetic shields within a Faraday cage.

second-order Doppler shift (see SM [26]). The numeric models are primarily used to quantify the dc Stark effect, but are also used to verify the accuracy of fitting line shapes with Eq. (2).

The ac Stark shift is our leading systematic, with typical shifts in the range of 50 to 300 kHz. To properly account for this effect, we drive the resonance with a range of intensities, quenching between 15% and 60% of the metastable population, and extrapolate to zero laser power. This extrapolation is similar to previous measurements of the $2S - nS/D$ transitions [19,20,36]. For each day of data collection, a single extrapolation is generated (an example is shown in Fig. 2).

The ac Stark effect introduces a shift in the resonance frequency of the $2S_{1/2} - 8D_{5/2}$ transition that is linear with intensity [37]. However, extrapolations on an ensemble of metastable atoms acquire a slight nonlinearity due to the different intensity profiles sampled by metastable atoms with different trajectories. As atoms following trajectories sampling the most intense portions of the 778 nm cavity mode begin to saturate, atoms along trajectories which sample lower intensities begin to contribute relatively more to the determination of the line center. This effect was present in the previous measurement of the $2S_{1/2} - 8D_{5/2}$ transition [19,20], though the nonlinearity present in our extrapolations is smaller due to the more stringent geometric constraints on the atomic trajectories in our apparatus.

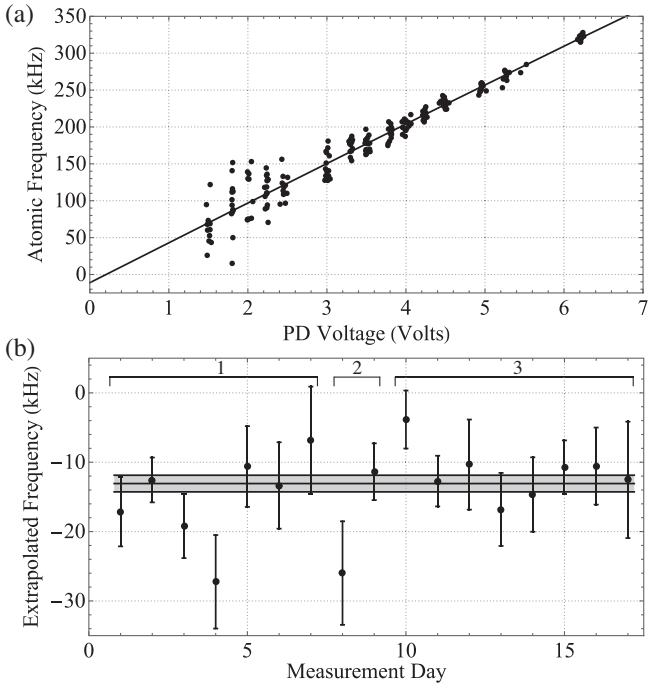

FIG. 2. (a) Example ac extrapolation data and cubic fit as a function of the 778 nm cavity transmission photodiode (PD) voltage. (b) Extrapolated zero-field frequencies for each measurement day with overall mean and statistical uncertainty overlaid. Data acquisition on the $2S_{1/2} - 8D_{5/2}$ transition was collected in batches grouped by date, which are indicated with batch numbers 1, 2, and 3. Frequencies in both (a) and (b) are relative to the value listed in Ref. [38].

While the nonlinearity is relatively small, ignoring it shifts the extrapolated resonance frequency by several kHz. Sampling an appreciable range of intracavity laser powers is required to properly determine the nonlinearity. From analytic considerations we have found that the nonlinearity acquired due to this spatial distribution is predominantly cubic and that this conclusion does not depend on the metastable spatial distribution (see SM [26]); both of these results are strongly supported by our numeric line shape models. Seventeen suitable extrapolations form the basis of our dataset and are shown in Fig. 2.

Our second leading systematic is due to the dc Stark effect, which leads to shifts and distortions of the $2S_{1/2} - 8D_{5/2}$ line. We have taken steps to passively mitigate stray fields by enclosing the entire metastable excitation and spectroscopic volume within a Faraday cage coated in colloidal graphite [41]. Because of the near degeneracy of the 8D, 8P, and 8F manifolds, the transition is very sensitive to static fields with shifts of $\sim 12\ \mathrm{kHz}/(\mathrm{V/m})^2$. Higher lying n manifolds are even more sensitive to the presence of static fields due to the narrower natural linewidths, increasing degeneracy of the states, and larger dipole matrix elements between the states. This makes the line distortions of transitions to higher n states a sensitive probe of the stray fields [19,20].

From measurements of the $2S_{1/2} - 12D_{5/2}$ line shape distortion, we have observed that the stray fields are stable day to day as long as the system remains under vacuum, and that the stray field orientation is parallel with the atomic beam. The orientation of the stray field was determined by varying the excitation light polarization and comparing the shift and distortion of the line. Between batches of data collection on the $2S_{1/2} - 8D_{5/2}$ line, the chamber was vented, leaving the possibility of stray field variation within the dataset. Therefore, we also measured the electric field strength for each day *in situ* by averaging several $2S_{1/2} - 8D_{5/2}$ scans from a single day and at similar 778 nm laser power. We then fit this averaged line with the numeric model to match the subtle line distortion and extract the stray dc field (see SM for additional detail [26]). Figure 3 shows the determined electric field for each measurement day. We find the average static field for each batch of data and use that field strength to determine the shift for that set of data.

The coupling introduced by the dc electric field causes a quadratic shift due to nearby dipole-allowed transitions and a line shape distortion due to the mixing between the nearly degenerate $8D_{5/2}$ and $8F_{5/2}$ states [20]. Since the lines are fit with the simple analytic function given in Eq. (2), the distortion also produces an additional shift. For each of the three measured electric fields shown in Fig. 3, the resulting

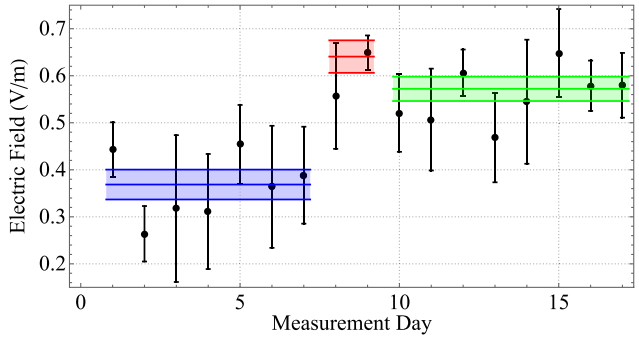

FIG. 3. Fit electric field for each measurement day, with data collection batch average overlaid.

dc Stark shift is determined with the numeric model. Then, the appropriate correction for each extrapolated resonance frequency in a given batch is applied. The three batches of electric field corrections are $-1.92(0.32)$, $-5.45(0.54)$, and $-4.43(0.37)$ kHz, respectively. Because of the statistical contribution of each batch to the final dataset, the weighted dc Stark correction for the entire measurement is $-3.54(0.37)$ kHz.

The correction of $-3.54(0.37)$ kHz assumes a stray field which is perpendicular to the spectroscopy light polarization. However, we cannot completely exclude a small parallel field, which can modify the required correction by up to 0.65 kHz. Additionally, from the numeric model, we find there is a small amount of cross talk between the ac extrapolation and dc Stark effect. This cross talk amounts to a -0.35 kHz correction to the dc Stark shift, and we assign the full 0.35 kHz shift as the associated uncertainty. Since the systematic shifts associated with the cross-talk effect, the possibility of nonperpendicular fields, and the statistical variance of the dc field correction are highly correlated, we combine their uncertainties linearly and obtain a net dc Stark correction of $-3.89(1.36)$ kHz.

We believe the vacuum pressure is limited by water, which has an intrinsic dipole moment. During a collision with a water molecule, a hydrogen atom experiences a varying electric field which can drive population in the 8D state to nearby states, quenching the 8D state and broadening the line [42]. We have employed Monte Carlo simulations of these H-H_2O collisions to estimate the shift and broadening, similar to Ref. [39]. From these simulations we have found that any associated pressure shifts are below the $\sim$1 Hz level and insignificant at our current level of precision.

Because of the two-photon excitation of the $2S_{1/2}-8D_{5/2}$ transition in an optical cavity, the first-order Doppler shift is effectively absent. The second-order Doppler shift remains, given by $\Delta\nu_{\mathrm{DS}} = -0.5(v/c)^2\nu$, for atomic velocity v. An advantage of our apparatus is the ability to directly characterize the hydrogen and metastable hydrogen velocity distributions via a time-of-flight measurement [21]. From such measurements, we have found the metastable velocity distribution is well approximated by $P(v) \propto v^4 e^{-\beta v^2}$, with $\beta = m/2k_bT$, and the required correction is $-0.73(0.10)$ kHz.

TABLE I. Minor corrections and uncertainties of the extrapolated $2S_{1/2} - 8D_{5/2}$ hyperfine centroid.

	$\Delta\nu$ (kHz)	σ (kHz)
Stark corrected	770 649 561 571.01	1.82
Second-order Doppler	0.73	0.10
Zeeman effect	0	0.56
Frequency calibration	−0.40	0.47
Blackbody radiation	−0.49	0.16
Pressure shifts	0	10^{-3}
$8D_{5/2}$ hyperfine structure	0	0.03
Photodiode imperfections	0	0.32
Incoherent line pulling	0	10^{-3}
Light force shift	0	10^{-3}
Total: Minor corrections	−0.16	0.82
Hyperfine centroid	770 649 561 570.9	2.0

From the ac extrapolation data, we recover a $2S_{1/2} - 8D_{5/2}$ hyperfine centroid of 770649561574.90(1.20) kHz. The dc Stark correction shifts this centroid by $-3.89(1.36)$ kHz to 770 649 561 571.01(1.82) kHz. We then apply minor corrections in our uncertainty budget as shown in Table I. A summary of the treatment of these corrections may be found in the SM [26]. With all the systematic corrections accounted for, we find a $2S_{1/2} - 8D_{5/2}$ resonance frequency of

$$\nu = 770649561570.9(2.0)\ \text{kHz}. \tag{3}$$

Combining our result with the $1S_{1/2} - 2S_{1/2}$ value [40], we obtain $r_p = 0.8584(51)$ fm, and $R_\infty = 10973731.568332(52)\ \text{m}^{-1}$. Our obtained r_p is presented alongside a selection of recent determinations of r_p from spectroscopic results in Fig. 4. Our value is 3.1 combined standard deviations from the latest CODATA recommended r_p value [43].

While the data shown in Fig. 4 combine the $1S_{1/2} - 2S_{1/2}$ measurement [40] with other hydrogen spectroscopy to extract r_p, it is also interesting to use the value of r_p determined from muonic hydrogen [14] as input data for Eq. (1). This is a compelling approach considering that a recent measurement of the Lamb shift in normal hydrogen is in agreement with the muonic result [17]. With that, a single measured interval in hydrogen is sufficient to extract R_∞. The result of this analysis for a selection of the most precise hydrogen laser spectroscopy data is shown in Fig. 5. The uncertainty for the Rydberg constant determination from the $1S_{1/2} - 2S_{1/2}$ transition shown in Fig. 5 is almost entirely due to the theoretical uncertainty of the 1S state. In order to avoid including this correlated uncertainty in

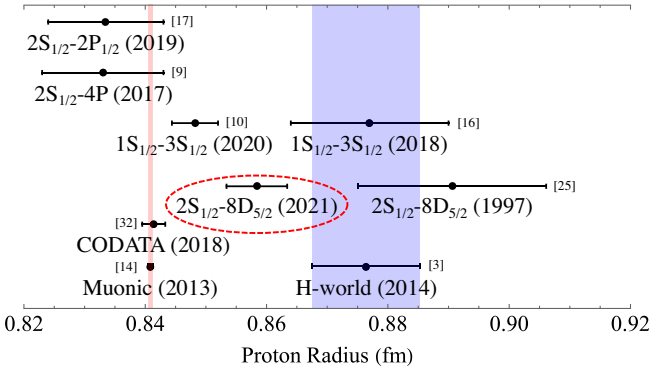

FIG. 4. A selection of recent determinations of the proton radius when combining laser spectroscopy with the $1S_{1/2} - 2S_{1/2}$ transition [9,10,16,19,40]. The result presented here is circled. The r_p denoted by H-world (2014) corresponds to the proton radius obtained in Ref. [3] using only hydrogen spectroscopy data (Adj. 8 Table XXIX). Also shown are the proton radius determinations from Lamb shift measurements in hydrogen [17] and muonic hydrogen [14], along with the most recent CODATA value [43].

the $1S_{1/2} - 3S_{1/2}$ determinations [10,16], we have subtracted the very precisely determined $1S_{1/2} - 2S_{1/2}$ transition frequency [40] to obtain $2S_{1/2} - 3S_{1/2}$ intervals.

As can be seen from Fig. 5, there is a general trend toward larger Rydberg constant when using experimentally determined intervals between states with larger n. It is interesting to note that hydrogen spectroscopy can provide a test for massive bosons that provide an additional coupling between the nucleus and electron [7,8]. Such bosons introduce a potential with finite range (a Yukawa

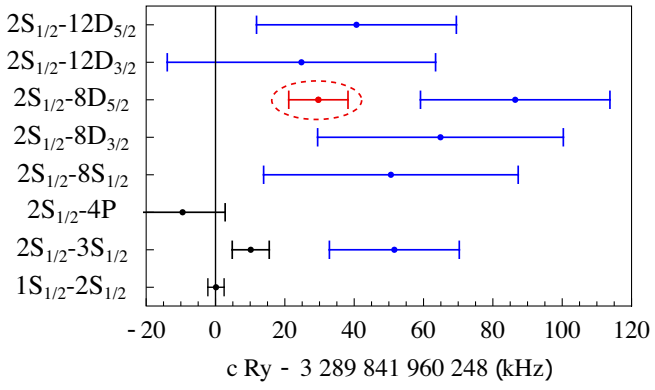

FIG. 5. A comparison of the Rydberg constant determined through Eq. (1) from one experimentally determined hydrogen interval. These determinations require a precise r_p value, which was taken from the muonic hydrogen measurement alone [14]. Blue points were measured in Paris (2S-3S [16], 2S-8S/D [19], 2S-12D [36]), black points were measured in Garching ($1S_{1/2} - 2S_{1/2}$ [40], $2S_{1/2} - 3S_{1/2}$ [10], $2S_{1/2} - 4P$ [9]), and our result is circled in red. As described in the text, we have subtracted the $1S_{1/2} - 2S_{1/2}$ interval [40] from the $1S_{1/2} - 3S_{1/2}$ measurements [10,16].

potential) which affects certain n states in hydrogen more strongly than others, producing an n dependence when extracting R_∞. As shown in the SM [26], the variation in Rydberg constant tends to decrease as the n of either the upper or lower state increases. We found that the reduced χ^2 for the data shown in Fig. 5 decreases from ~4.0 to ~2.0 with the addition of a Yukawa potential with a length scale of $\sim 34 a_0$. Therefore, while the perturbation from such a potential can drastically reduce the inconsistency within the dataset shown in Fig. 5, it does not eliminate it.

Future investigations of $2S - nS/D$ transitions in hydrogen are attractive due to the narrow natural lines afforded by such states and the convenience of the laser wavelengths required to drive the transitions. Additionally, the current n dependence of the Rydberg constant extractions as shown in Fig. 5 provides a compelling case for further measurements of transitions to relatively high n as a search for new physics [7,8].

We gratefully acknowledge useful conversations with J. Berger, S. M. Brewer, A. Grinin, S. A. Lee, L. Maisenbacher, R. Pohl, J. L. Roberts, Th. Udem, and V. Wirthl. We would like to thank the NIST WWVB team for accommodating our check of the GPS-disciplined Rb time standard as described in the Letter. Finally, we gratefully acknowledge funding for this measurement through the NIST Precision Measurement Grant (60NANB16D270), and the NSF CAREER Program (1654425).

*dylan.yost@colostate.edu

[1] S. G. Karshenboim, Precision physics of simple atoms: QED tests, nuclear structure and fundamental constants, Phys. Rep. **422**, 1 (2005).
[2] S. G. Karshenboim, F. S. Pavone, G. F. Bassani, M. Inguscio, and T. W. Hänsch, *Introduction to Simple Atoms* (Springer, New York, 2007).
[3] P. J. Mohr, D. B. Newell, and B. N. Taylor, CODATA recommended values of the fundamental physical constants: 2014*, Rev. Mod. Phys. **88**, 035009 (2016).
[4] S. G. Karshenboim and V. G. Ivanov, Hyperfine structure of the ground and first excited states in light hydrogen-like atoms and high-precision tests of QED, Eur. Phys. J. D **19**, 13 (2002).
[5] M. S. Safronova, D. Budker, D. Demille, D. F. Kimball, A. Derevianko, and C. W. Clark, Search for new physics with atoms and molecules, Rev. Mod. Phys. **90**, 025008 (2018).
[6] L. C. Tu and J. Luo, Experimental tests of Coulomb's law and the photon rest mass, Metrologia **41**, S136 (2004).
[7] S. G. Karshenboim, Precision Physics of Simple Atoms and Constraints on a Light Boson with Ultraweak Coupling, Phys. Rev. Lett. **104**, 220406 (2010).
[8] M. P. A. Jones, R. M. Potvliege, and M. Spannowsky, Probing new physics using Rydberg states of atomic hydrogen, Phys. Rev. Research **2**, 013244 (2020).
[9] A. Beyer, L. Maisenbacher, A. Matveev, R. Pohl, K. Khabarova, A. Grinin, T. Lamour, D. C. Yost, T. W. Hänsch,

N. Kolachevsky, and T. Udem, The Rydberg constant and proton size from atomic hydrogen, Science **358**, 79 (2017).
[10] A. Grinin, A. Matveev, D. C. Yost, L. Maisenbacher, V. Wirthl, R. Pohl, T. W. Hänsch, and T. Udem, Two-photon frequency comb spectroscopy of atomic hydrogen, Science **370**, 1061 (2020).
[11] M. Horbatsch and E. A. Hessels, Tabulation of the bound-state energies of atomic hydrogen, Phys. Rev. A **93**, 022513 (2016).
[12] R. Pohl *et al.*, The size of the proton, Nature (London) **466**, 213 (2010).
[13] A. Antognini *et al.*, Proton structure from the measurement of 2S-2P transition frequencies of muonic hydrogen, Science **339**, 417 (2013).
[14] R. Pohl, R. Gilman, G. A. Miller, and K. Pachucki, Muonic hydrogen and the proton radius puzzle, Annu. Rev. Nucl. Part. Sci. **63**, 175 (2013).
[15] C. E. Carlson, The proton radius puzzle, Prog. Part. Nucl. Phys. **82**, 59 (2015).
[16] H. Fleurbaey, S. Galtier, S. Thomas, M. Bonnaud, L. Julien, F. Biraben, F. Nez, M. Abgrall, and J. Guéna, New Measurement of the 1*S*–3*S* Transition Frequency of Hydrogen: Contribution to the Proton Charge Radius Puzzle, Phys. Rev. Lett. **120**, 183001 (2018).
[17] N. Bezginov, T. Valdez, M. Horbatsch, A. Marsman, A. C. Vutha, and E. A. Hessels, A measurement of the atomic hydrogen Lamb shift and the proton charge radius, Science **365**, 1007 (2019).
[18] F. Biraben, J. C. Garreau, and L. Julien, Détermination of the Rydberg constant by Doppler-free two-photon spectroscopy of hydrogen Rydberg states, Europhys. Lett. **2**, 925 (1986).
[19] B. De Beauvoir, F. Nez, L. Julien, B. Cagnac, F. Biraben, D. Touahri, L. Hilico, O. Acef, A. Clairon, and J. J. Zondy, Absolute Frequency Measurement of the $2S - 8S/D$ Transitions in Hydrogen and Deuterium: New Determination of the Rydberg Constant, Phys. Rev. Lett. **78**, 440 (1997).
[20] B. De Beauvoir, C. Schwob, O. Acef, L. Jozefowski, L. Hilico, F. Nez, L. Julien, A. Clairon, and F. Biraben, Metrology of the hydrogen and deuterium atoms: Determination of the Rydberg constant and Lamb shifts, Eur. Phys. J. D **12**, 61 (2000).
[21] S. F. Cooper, A. D. Brandt, C. Rasor, Z. Burkley, and D. C. Yost, Cryogenic atomic hydrogen beam apparatus with velocity characterization, Rev. Sci. Instrum. **91**, 013201 (2020).
[22] Z. Burkley, A. D. Brandt, C. Rasor, S. F. Cooper, and D. C. Yost, Highly coherent, watt-level deep-UV radiation via a frequency-quadrupled Yb-fiber laser system, Appl. Opt. **58**, 1657 (2019).
[23] S. F. Cooper, Z. Burkley, A. D. Brandt, C. Rasor, and D. C. Yost, Cavity-enhanced deep ultraviolet laser for two-photon cooling of atomic hydrogen, Opt. Lett. **43**, 1375 (2018).
[24] M. A. Lombardi, The use of GPS disciplined oscillators as primary frequency standards for calibration and metrology laboratories, NCSLI Meas. **3**, 56 (2008).
[25] T. Udem, L. Maisenbacher, A. Matveev, V. Andreev, A. Grinin, A. Beyer, N. Kolachevsky, R. Pohl, D. C. Yost, and T. W. Hänsch, Quantum Interference Line Shifts of Broad Dipole-Allowed Transitions, Ann. Phys. (Amsterdam) **531**, 1900044 (2019).
[26] See Supplemental Material at http://link.aps.org/supplemental/10.1103/PhysRevLett.128.023001 for details related to the data analysis, systematic shifts, and the effects of a Yukawa potential on the extraction of the Rydberg constant, which includes Refs. [8–10,16,19–21, 24,25,27–40].
[27] J. W. Farley and W. H. Wing, Accurate calculation of dynamic Stark shifts and depopulation rates of Rydberg energy levels induced by blackbody radiation. Hydrogen, helium, and alkali-metal atoms, Phys. Rev. A **23**, 2397 (1981).
[28] S. A. Clough, Y. Beers, G. P. Klein, and L. S. Rothman, Dipole moment of water from Stark measurements of H22O, HDO, and D2O, J. Chem. Phys. **59**, 2254 (1973).
[29] J. Cooper, Broadening of isolated lines in the impact approximation using a density matrix formulation, Rev. Mod. Phys. **39**, 167 (1967).
[30] I. I. Sobel'man, *An Introduction to the Theory of Atomic Spectra* (Pergamon Press, New York, 1972).
[31] R. A. Swainson and G. W. F. Drake, A unified treatment of the non-relativistic and relativistic hydrogen atom: III. The reduced Green functions, J. Phys. A **24**, 1801 (1991).
[32] H. A. Bethe and E. E. Salpeter, *Quantum Mechanics of One- and Two-Electron Atoms*, 1st ed. (Springer-Verlag, Berlin, 1957).
[33] M. Horbatsch and E. A. Hessels, Shifts from a distant neighboring resonance, Phys. Rev. A **82**, 052519 (2010).
[34] D. C. Yost, A. Matveev, E. Peters, A. Beyer, T. W. Hänsch, and T. Udem, Quantum interference in two-photon frequency-comb spectroscopy, Phys. Rev. A **90**, 012512 (2014).
[35] H. Fleurbaey, F. Biraben, L. Julien, J. P. Karr, and F. Nez, Cross-damping effects in 1S-3S spectroscopy of hydrogen and deuterium, Phys. Rev. A **95**, 052503 (2017).
[36] C. Schwob, L. Jozefowski, B. De Beauvoir, L. Hilico, F. Nez, L. Julien, F. Biraben, O. Acef, and A. Clairon, Optical Frequency Measurement of the $2S - 12D$ Transitions in Hydrogen and Deuterium: Rydberg Constant and Lamb Shift Determinations, Phys. Rev. Lett. **82**, 4960 (1999).
[37] M. Haas, U. D. Jentschura, C. H. Keitel, N. Kolachevsky, M. Herrmann, P. Fendel, M. Fischer, T. Udem, R. Holzwarth, T. W. Hänsch, M. O. Scully, and G. S. Agarwal, Two-photon excitation dynamics in bound two-body Coulomb systems including ac Stark shift and ionization, Phys. Rev. A **73**, 052501 (2006).
[38] A. E. Kramida, A critical compilation of experimental data on spectral lines and energy levels of hydrogen, deuterium, and tritium, At. Data Nucl. Data Tables **96**, 586 (2010).
[39] A. Matveev, N. Kolachevsky, C. M. Adhikari, and U. D. Jentschura, Pressure shifts in high-precision hydrogen spectroscopy: II. Impact approximation and Monte-Carlo simulations, J. Phys. B At. Mol. Opt. Phys. **52**, 75006 (2019).
[40] C. G. Parthey, A. Matveev, J. Alnis, B. Bernhardt, A. Beyer, R. Holzwarth, A. Maistrou, R. Pohl, K. Predehl, T. Udem,

T. Wilken, N. Kolachevsky, M. Abgrall, D. Rovera, C. Salomon, P. Laurent, and T. W. Hänsch, Improved Measurement of the Hydrogen 1*S*–2*S* Transition Frequency, Phys. Rev. Lett. **107**, 203001 (2011).

[41] B. H. Porter, Research applications of colloidal graphite, Rev. Sci. Instrum. **7**, 101 (1936).

[42] I. I. Sobel'man, L. A. Vainshtein, and A. Y. Evgenii, *Excitation of Atoms and Broadening of Spectral Lines* (Springer-Verlag, Berlin, 1955).

[43] E. Tiesinga, P. J. Mohr, D. B. Newell, and B. N. Taylor, Codata recommended values of the fundamental physical constants: 2018, Rev. Mod. Phys. **93**, 025010 (2021).